Supplement of Atmos. Chem. Phys., 24, 6769–6786, 2024
https://doi.org/10.5194/acp-24-6769-2024-supplement
© Author(s) 2024. CC BY 4.0 License.

Atmospheric Chemistry and Physics
Open Access
EGU

Supplement of

Investigating the contribution of grown new particles to cloud condensation nuclei with largely varying preexisting particles – Part 2: Modeling chemical drivers and 3-D new particle formation occurrence

Ming Chu et al.

Correspondence to: Yang Gao (yanggao@ouc.edu.cn) and Xiaohong Yao (xhyao@ouc.edu.cn)

The copyright of individual parts of the supplement might differ from the article licence.

Figure legends:

Fig. S1 Time series of simulated and observed particle mass concentrations of SO_4^{2-} (a), NO_3^- (b), NH_4^+ (c) and organics (d) in $PM_{1.0}$ at an urban site (39.98ºN, 116.39ºE) in Beijing from June 23 to July 14 and the comparison between the simulated and observed SO_4^{2-} (e), NO_3^- (f), NH_4^+ (g) and organics (h) during the frequent-NPF period of June 29–July 6 (the MFB, MFE and R in parentheses are calculated with the data excluding July 5, empty symbols in e-h represent the data on July 5).

Fig. S2 Time series of the observed and modeled $PM_{2.5}$ mass concentrations from June 23 to July 14 in Beijing downtown (a: 39.86°N, 116.36°E) and Beijing suburb (b: 40.19°N, 116.23°E), the comparison of the modeled and observed $PM_{2.5}$ during the frequent-NPF period in Beijing downtown (c) and Beijing suburb (d, the MFB, MFE and R in parentheses are calculated with the data excluding July 5).

Fig. S3 Simulated concentrations of H_2SO_4 vapor on July 1–2 and the ranges of observational values reported in the literature (Two endpoints reported by Lu et al. (2019) and Wang et al. (2021) represent the maximum and minimum values, respectively).

Fig. S4 Diurnal variations in modeled chemical components in 10–40 nm particles and 40–250 nm particles: (a) SO_4^{2-}, (b) NO_3^-, (c) NH_4^+ (d) organics on July 3–4; fractions of chemical species in 10–40 nm particles at 15:00 (e), in 40–250 nm particles at 15:00 (f), in 10–40 nm particles at 22:00 (g), and in 40–250 nm particles at 22:00 on July 3.

Fig. S5 Diurnal variation in modeled chemical components in 10–40 nm particles and 40–250 nm particles: SO_4^{2-} (a), NO_3^- (b), NH_4^+ (c), organics (d) on July 6–7; fractions of chemical species in 10–40 nm particles (e) and 40–250 nm particles (f) at 12:00, those at 17:00 (g and h) and those at 22:00 on July 6 (i and j).

Fig. S6 Comparison of the simulations with observations of CCN number concentration during the NPF events on July 1, 3, 6 at 0.2 % SS (a–c) and 0.4 % SS (d–f) (a and d on July 1; b and e on July 3; c and f on July 6).

Fig. S7 The simulated chemical components in 10–40 nm particles at 500 m, 1500 m and 2500 m above the ground respectively at 10:00 (a), 15:00 (b), 22:00 (c) on July 3 and 3:00 (d) on July 4.

Fig. S8 The simulated chemical components in 10–40 nm particles at 500 m, 1500 m and 2500 m above the ground respectively at 12:00 (a), 15:00 (b), 18:00 (c) on July 6.

Fig. S9 Horizontal distributions of CN_{10} at ~1300 m a.s.l. (a, the upper row) and on the ground level (a, the bottom row) at 08:00, 09:00, 12:00, 17:00 and 18:00 on July 3, 2019 (red and blue solid dots represent the observation site and point A, respectively; the direction and length of black arrow represent the wind direction and wind speed, respectively); Vertical profiles of CN_{10} over the observation site (red solid line) and point A (blue dashed line) from 0:00 to 22:00 on 3 July 2019 (b, the Y-axis coordinate is the height above ground; the red and blue solid dots represent the height of the PBL over the observation site and point A, and PBL exceeding 3000 meters above ground are not shown in Figure).

Fig. S10 Horizontal distribution of CN_{10} at ~1300 m a.s.l. (a, the upper row) and on ground (a, the bottom row) in NPF event occurred on July 6, 2019 at 10:00, 11:00, 14:00, 17:00 and 18:00 (the red and blue solid dots represent the observation site and point A, respectively; the direction and size of the black arrow represent the wind direction and wind speed, respectively); Vertical profiles of CN_{10} over the observational site (red solid line) and point A (blue dashed line) from 0:00 to 22:00 on July 6, 2019 (b, the Y-axis coordinate is the height above the ground; the red and blue solid dots represent the height of the PBL over the observational site and point A, and PBL exceeding 3000 meters above the ground are not shown in Figure).

Fig. S11 Horizontal distribution of CN_{40-250} on ground (a, the upper row) and vertical profiles of CN_{40-250} over the observation site (red solid line), point A (blue dashed line) and point B (black dashed line) from 18:00 on July 3 to 04:00 on July 4 (b, the Y-axis coordinate is the height above the ground; the red, blue and black solid dots represent the height of the PBL over the observation site, point A and point B, and PBL exceeding 3000 meters above the ground are not shown in Figure).

Table legends:

Table S1. Parameter scheme setting in WRF-Chem model

1 **Figures**

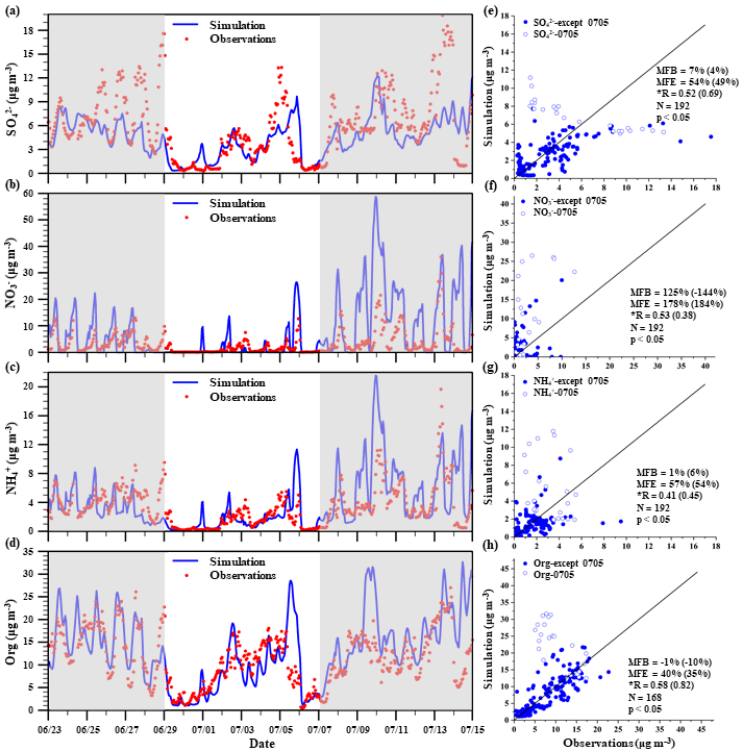

2

3 **Fig. S1**

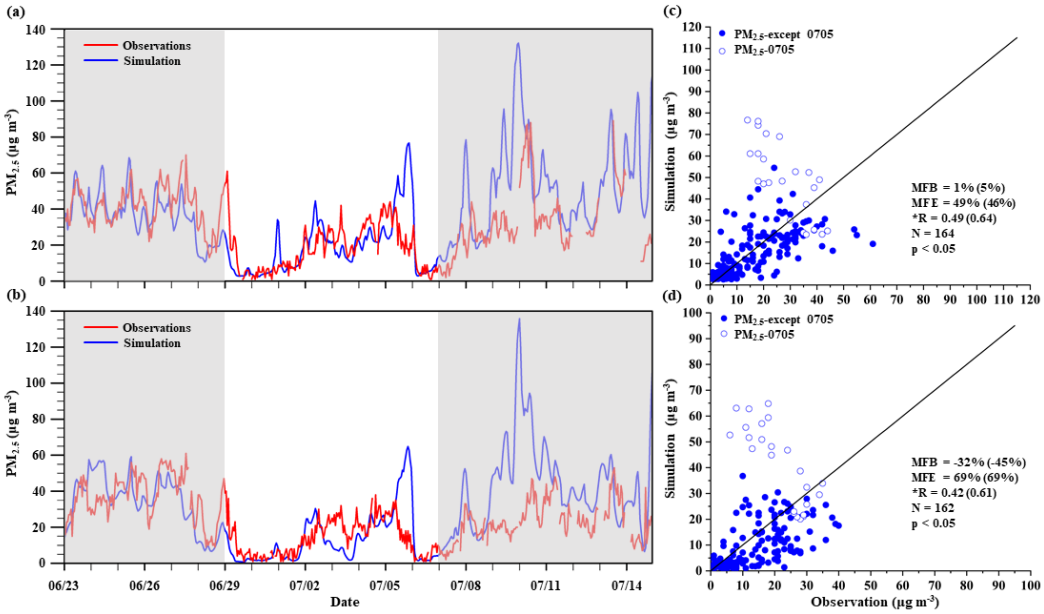
(a)
Observations
Simulation
PM2.5 (μg m-3)
(b)
Observations
Simulation
PM2.5 (μg m-3)
06/23
06/26
06/29
07/02
07/05
07/08
07/11
07/14
Date
(c)
PM2.5-except 0705
PM2.5-0705
Simulation (μg m-3)
MFB = 1% (5%)
MFE = 49% (46%)
*R = 0.49 (0.64)
N = 164
p < 0.05
(d)
PM2.5-except 0705
PM2.5-0705
Simulation (μg m-3)
MFB = -32% (-45%)
MFE = 69% (69%)
*R = 0.42 (0.61)
N = 162
p < 0.05
Observation (μg m-3)

Fig. S2

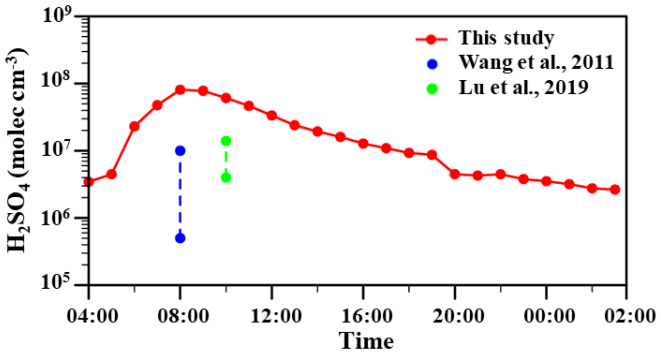
This study
Wang et al., 2011
Lu et al., 2019
H_2SO_4 (molec cm^{-3})
10^9
10^8
10^7
10^6
10^5
04:00
08:00
12:00
16:00
20:00
00:00
02:00
Time

Fig. S3

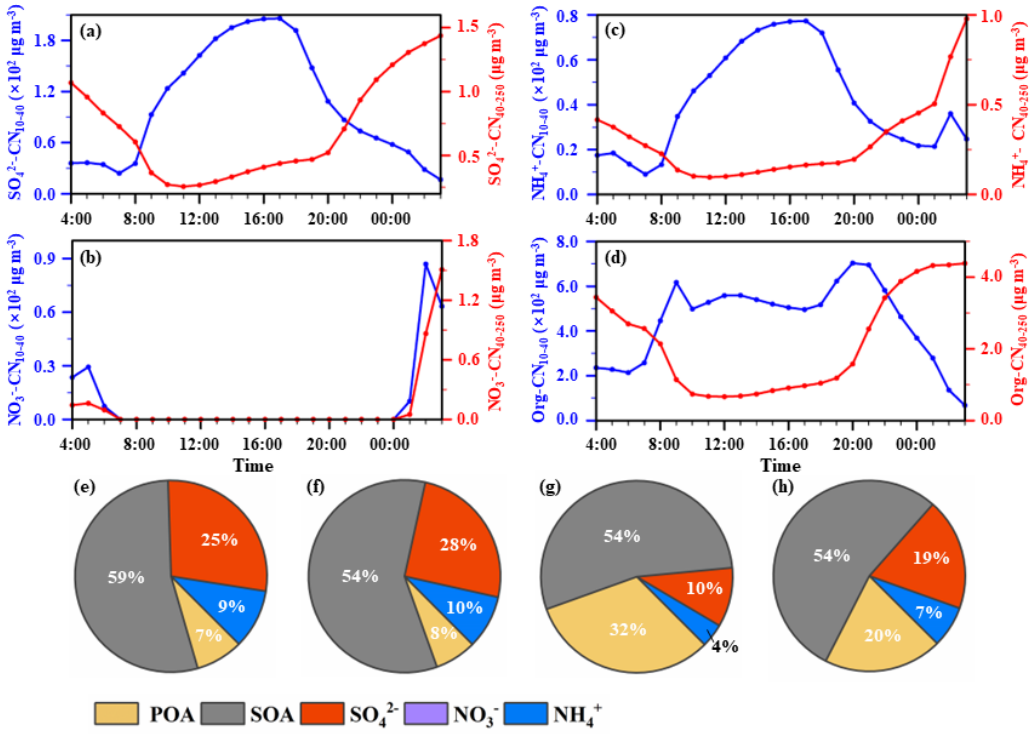
(a)
(b)
(c)
(d)
(e)
(f)
(g)
(h)
Time
4:00
8:00
12:00
16:00
20:00
00:00
25%
59%
9%
7%
28%
54%
10%
8%
54%
10%
32%
4%
54%
19%
7%
20%
POA
SOA
SO4 2-
NO3 -
NH4 +

Fig. S4

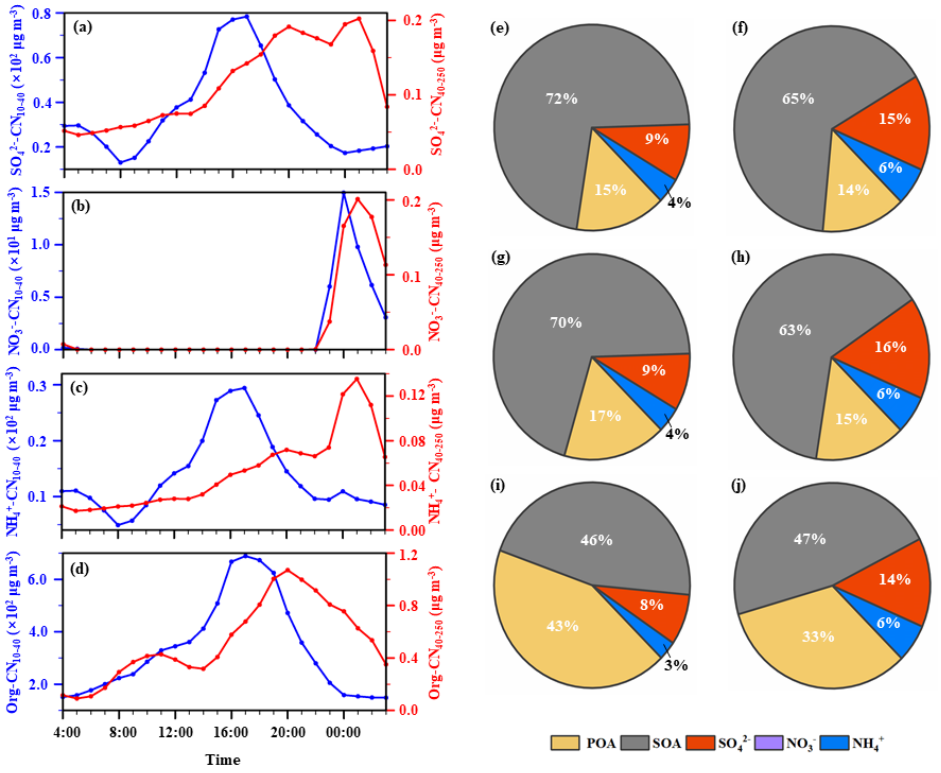
(a)
(b)
(c)
(d)
(e)
(f)
(g)
(h)
(i)
(j)
72%
9%
15%
4%
65%
15%
6%
14%
70%
9%
17%
4%
63%
16%
6%
15%
46%
8%
43%
3%
47%
14%
6%
33%
4:00
8:00
12:00
16:00
20:00
00:00
Time
POA
SOA
SO4 2-
NO3-
NH4+

Fig. S5

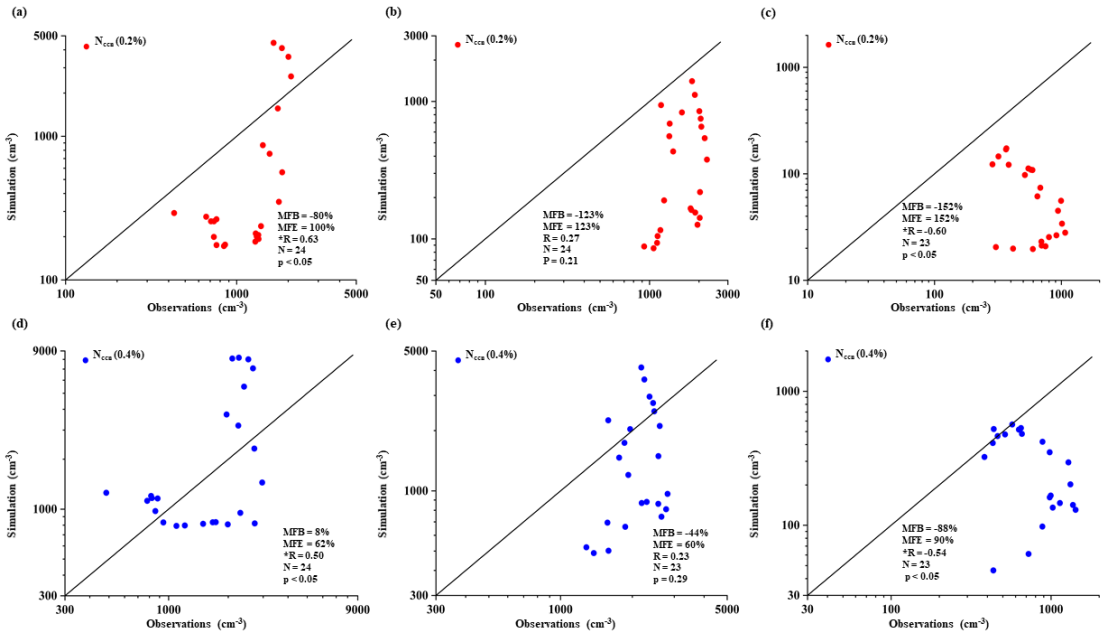
(a)
N_{ccn} (0.2%)
MFB = -80%
MFE = 100%
*R = 0.63
N = 24
p < 0.05
(b)
N_{ccn} (0.2%)
MFB = -123%
MFE = 123%
R = 0.27
N = 24
P = 0.21
(c)
N_{ccn} (0.2%)
MFB = -152%
MFE = 152%
*R = -0.60
N = 23
p < 0.05
(d)
N_{ccn} (0.4%)
MFB = 8%
MFE = 62%
*R = 0.50
N = 24
p < 0.05
(e)
N_{ccn} (0.4%)
MFB = -44%
MFE = 60%
R = 0.23
N = 23
p = 0.29
(f)
N_{ccn} (0.4%)
MFB = -88%
MFE = 90%
*R = -0.54
N = 23
p < 0.05
Simulation (cm^{-3})
Observations (cm^{-3})

Fig. S6

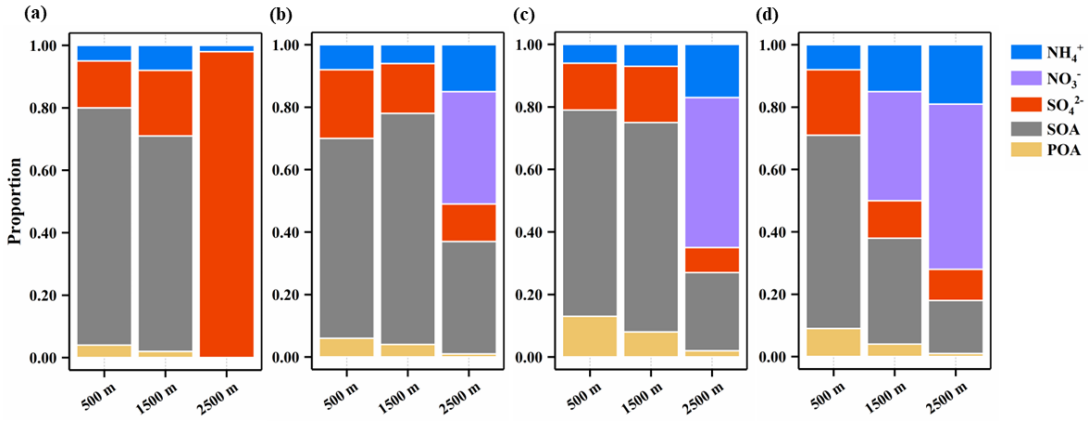
(a)
(b)
(c)
(d)
Proportion
1.00
0.80
0.60
0.40
0.20
0.00
500 m
1500 m
2500 m
NH4+
NO3-
SO42-
SOA
POA

Fig. S7

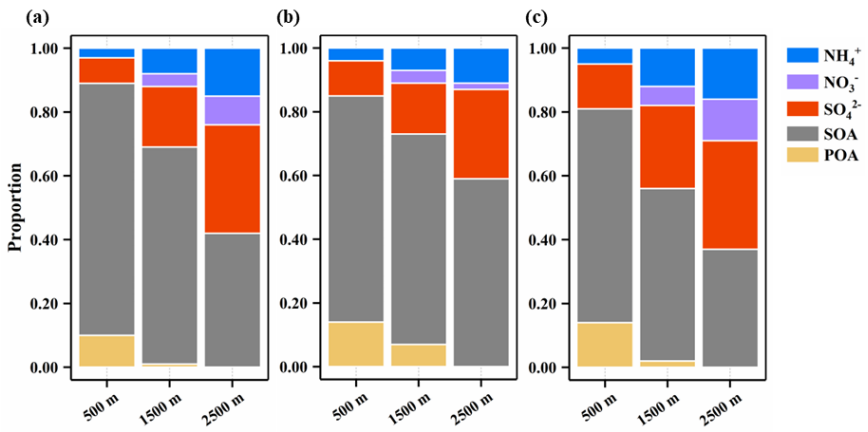
(a)
(b)
(c)
Proportion
1.00
0.80
0.60
0.40
0.20
0.00
500 m
1500 m
2500 m
NH4+
NO3-
SO42-
SOA
POA

Fig. S8

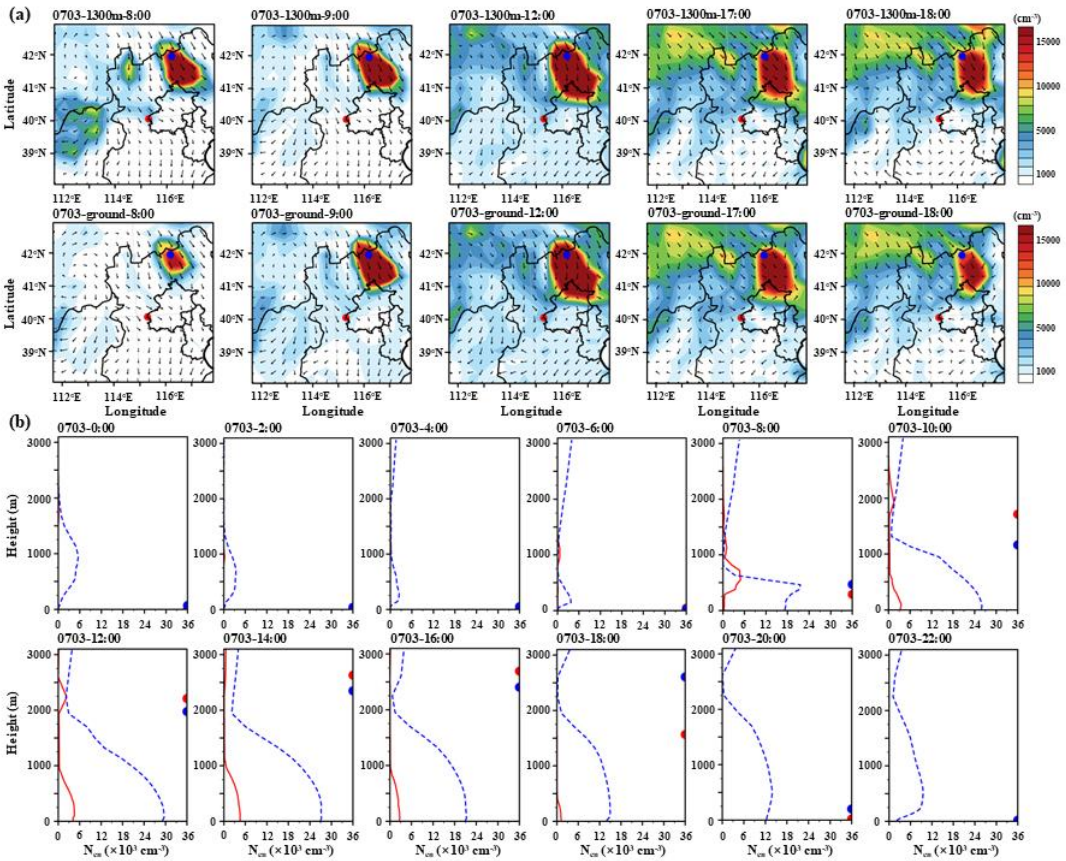
(a)
0703-1300m-8:00
0703-1300m-9:00
0703-1300m-12:00
0703-1300m-17:00
0703-1300m-18:00
0703-ground-8:00
0703-ground-9:00
0703-ground-12:00
0703-ground-17:00
0703-ground-18:00
Latitude
Longitude
(cm⁻³)
(b)
0703-0:00
0703-2:00
0703-4:00
0703-6:00
0703-8:00
0703-10:00
0703-12:00
0703-14:00
0703-16:00
0703-18:00
0703-20:00
0703-22:00
Height (m)
N_cn (×10³ cm⁻³)

Fig. S9

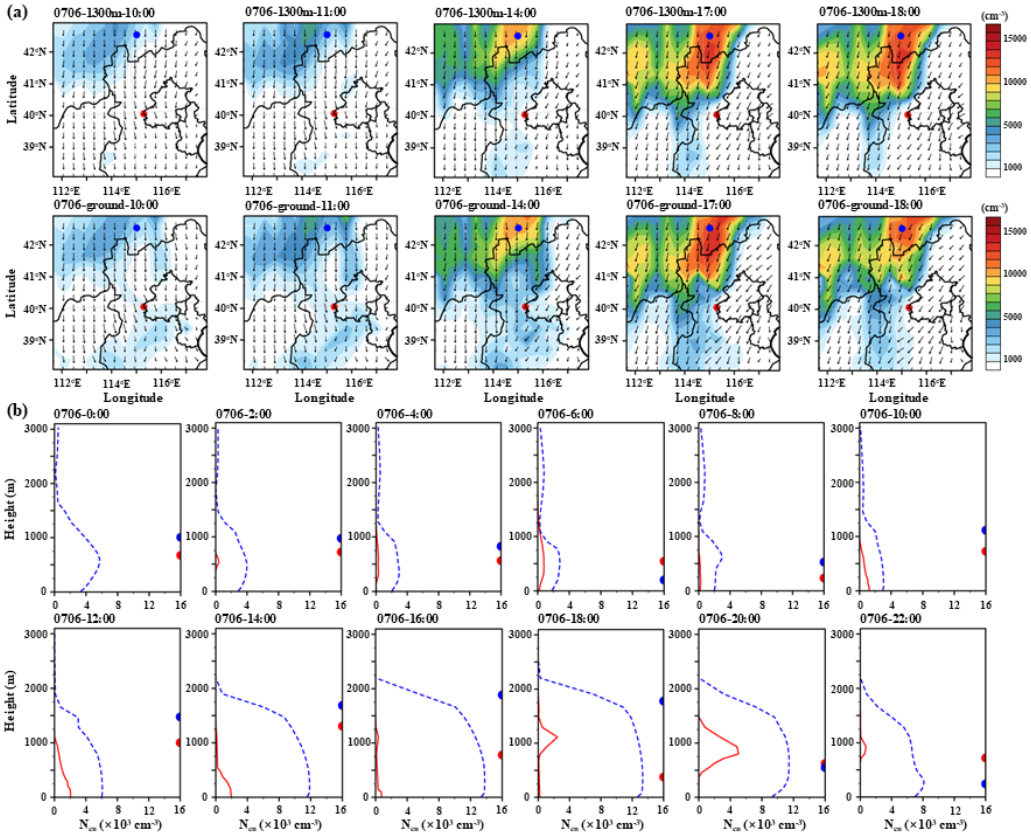
(a)
0706-1300m-10:00
0706-1300m-11:00
0706-1300m-14:00
0706-1300m-17:00
0706-1300m-18:00
0706-ground-10:00
0706-ground-11:00
0706-ground-14:00
0706-ground-17:00
0706-ground-18:00
Latitude
Longitude
(cm⁻³)
(b)
0706-0:00
0706-2:00
0706-4:00
0706-6:00
0706-8:00
0706-10:00
0706-12:00
0706-14:00
0706-16:00
0706-18:00
0706-20:00
0706-22:00
Height (m)
N_cn (×10³ cm⁻³)

Fig. S10

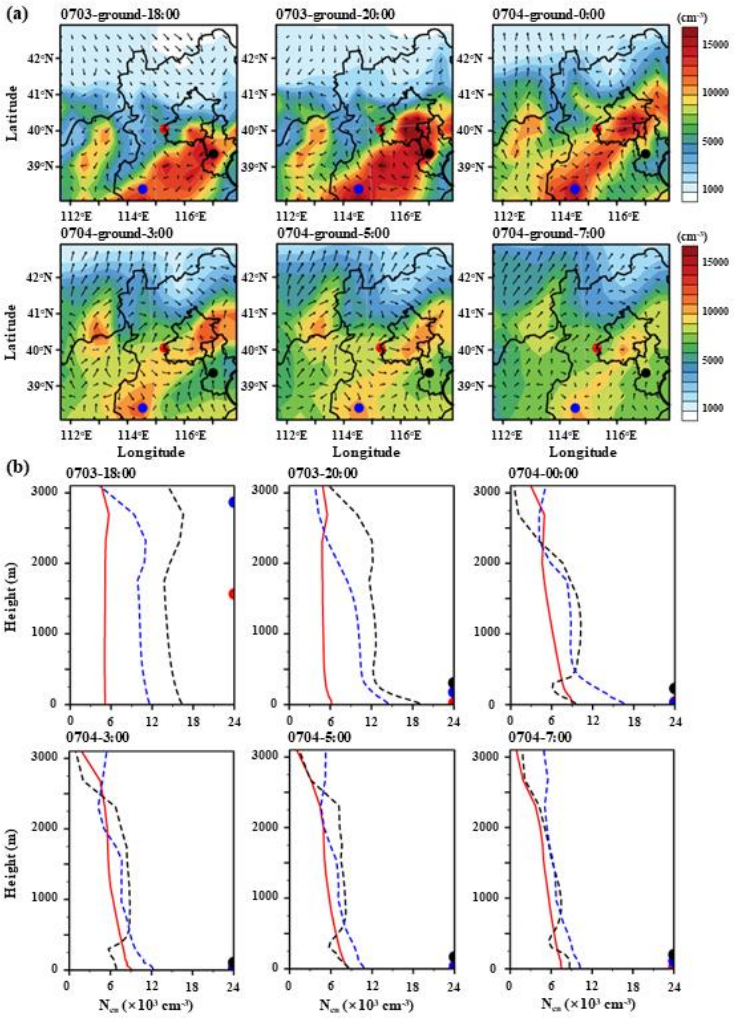
(a)
0703-ground-18:00
0703-ground-20:00
0704-ground-0:00
0704-ground-3:00
0704-ground-5:00
0704-ground-7:00
(cm⁻³)
15000
10000
5000
1000
Latitude
Longitude
42°N
41°N
40°N
39°N
112°E
114°E
116°E
(b)
0703-18:00
0703-20:00
0704-00:00
0704-3:00
0704-5:00
0704-7:00
Height (m)
3000
2000
1000
0
6
12
18
24
N_cn (×10³ cm⁻³)

Fig. S11

Table

Table S1 Parameter scheme setting in WRF-Chem model

Atmospheric process	Model scheme
Meteorological process	
Longwave radiation	RRTMG (Iacono et al., 2008)
Shortwave radiation	RRTMG (Iacono et al., 2008)
Land surface model	Unified Noah LSM (Tewari et al., 2016)
PBL scheme	YSU (Tewari et al., 2016)
Cumulus	Grell 3D (Grell and Dévényi, 2002)
Micro Physics	Morrision 2-moment (Morrison et al., 2009)
Chemical process	
Gas-phase chemistry	SAPRC99 (Carter, 2000)
Photolysis	Madronich F-TUV (Madronich, 1987)
Aerosol chemistry	MOSAIC (Zaveri et al., 2008)
Anthropogenic	Modified MEIC2016
Biogenic emissions	MEGAN v2.03

References

Carter, W.: Additions And Corrections To The Saprc-99 Maximum Incremental Reactivity (mir) Scale, 2000.

Grell, G. A. and Dévényi, D.: A generalized approach to parameterizing convection combining ensemble and data assimilation techniques, Geophys. Res. Lett., 29, 38-31-38-34, https://doi.org/10.1029/2002GL015311, 2002.

Iacono, M. J., Delamere, J. S., Mlawer, E. J., Shephard, M. W., Clough, S. A., and Collins, W. D.: Radiative forcing by long-lived greenhouse gases: Calculations with the AER radiative transfer models, J. Geophys. Res., 113, D13103, https://doi.org/10.1029/2008JD009944, 2008.

Lu, Y. Q., Yan, C., Fu, Y. Y., Chen, Y., Liu, Y. L., Yang, G., Wang, Y. W., Bianchi, F., Chu, B. W., Zhou, Y., Yin, R. J., Baalbaki, R., Garmash, O., Deng, C. J., Wang, W. G., Liu, Y. C., Petaja, T., Kerminen, V. M., Jiang, J. K., Kulmala, M., and Wang, L.: A proxy for atmospheric daytime gaseous sulfuric acid concentration in urban Beijing, Atmos. Chem. Phys., 19, 1971-1983, 10.5194/acp-19-1971- 2019, 2019.

Madronich, S.: Photodissociation in the atmosphere: 1. Actinic flux and the effects of ground reflections and clouds, J. Geophys. Res., 92, 9740-9752, https://doi.org/10.1029/JD092iD08p09740, 1987.

Morrison, H., Thompson, G., and Tatarskii, V.: Impact of Cloud Microphysics on the Development of Trailing Stratiform Precipitation in a Simulated Squall Line: Comparison of One- and Two-Moment Schemes, Mon. Weather. Rev., 137, 991-1007, https://doi.org/10.1175/2008MWR2556.1, 2009.

Tewari, M., Chen, F., Wang, W., Dudhia, J., and Cuenca, R. H.: Implementation and verification of the united NOAH land surface model in the WRF model, 20th Conference on Weather Analysis and Forecasting/16th Conference on Numerical Weather Prediction,

Wang, Z. B., Hu, M., Yue, D. L., Zheng, J., Zhang, R. Y., Wiedensohler, A., Wu, Z. J., Nieminen, T., and Boy, M.: Evaluation on the role of sulfuric acid in the mechanisms of new particle formation for Beijing case, Atmos. Chem. Phys., 11, 12663-12671, 10.5194/acp-11-12663-2011, 2011.

Zaveri, R. A., Easter, R. C., Fast, J. D., and Peters, L. K.: Model for Simulating Aerosol Interactions and Chemistry (MOSAIC), Journal of Geophysical Research Atmospheres, 113, https://doi.org/10.1029/2007JD008782, 2008.